8-2020

Kinetics, Affinity, Thermodynamics, and Selectivity of Phosphate Removal Using Immobilized Phosphate-Binding Proteins

Kaushik Venkiteshwaran

Erin Wells

Brooke Mayer

Environmental Science & Technology, Vol. 54, No. 17 (2020, August): 10885-10894. DOI.

Kinetics, Affinity, Thermodynamics, and Selectivity of Phosphate Removal Using Immobilized Phosphate-Binding Proteins

Kaushik Venkiteshwaran
Department of Civil, Construction and Environmental Engineering Marquette University, Milwaukee, Wisconsin
Erin Wells
Department of Civil, Construction and Environmental Engineering Marquette University, Milwaukee, Wisconsin
Brooke Mayer
Department of Civil, Construction and Environmental Engineering Marquette University, Milwaukee, Wisconsin

Abstract

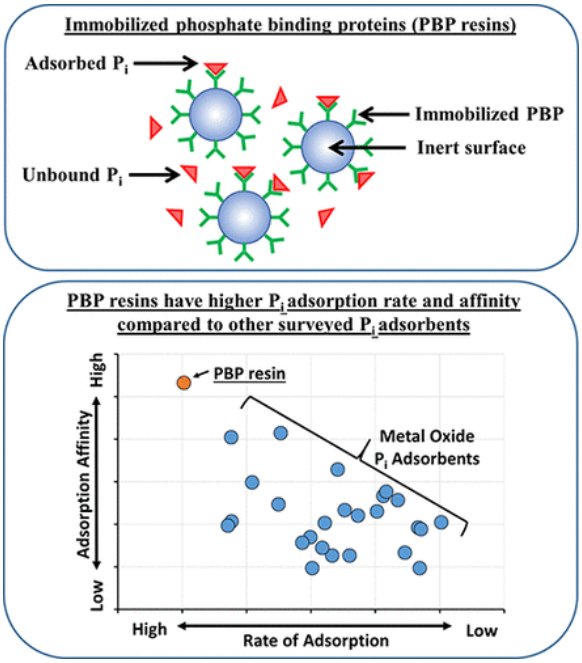

A phosphate (P_i)-selective adsorption system featuring immobilized P_i-binding proteins (PBP) has recently attracted attention for ultralow P_i removal followed by recovery. This study investigated the adsorption kinetics, affinity, thermodynamics, and selectivity, as well as the effect of pH and temperature on P_i adsorption using immobilized PBP (PBP resin). Immobilizing PBP did not affect its P_i affinity. Kinetic studies at 22 °C and pH 7.1 showed that the PBP resin achieved 95% of its equilibrium capacity within 0.64 ± 0.2 min. The estimated Langmuir affinity constant (K_L) was 21 ± 5 μM^{-1} P_i (220 ± 52 L/mg-P_i), which is higher than P_i adsorbents recently reported in literature. The ideal operating ranges for high-affinity P_i adsorption using PBP resin were pH 4.5 to 9 and temperature 14 to 37 °C. The P_i-PBP resin adsorption process was not affected by the presence of common anions (Cl^-, Br^-, NO_2^-, NO_3^-, SO_4^{2-}, and HCO_3^-). Adsorption using the P_i-PBP resin was exothermic (ΔH = −6.3 ± 1.3 kJ/mol) and spontaneous (ΔG = −39.7 ± 0.1 to −43.2 ± 0.2 kJ/mol) between 14 and 43 °C. These results indicate that PBP resin's P_i adsorption rate and affinity surpass those of existing adsorbents. Future work to increase the PBP resin's adsorption capacity is important to its application as a viable P_i adsorbent.

1. Introduction

Global concern over the economic and environmental damages caused by phosphorus (P)-based eutrophication of surface waters has intensified in recent decades.(1,2) In order to combat the problem, the United States Environmental Protection Agency (USEPA) suggests a mean total phosphorus (TP) concentration of 10 µg-P/L for lakes and reservoirs.(3) Given the risk of P pollution, regulations of point sources like treated sewage effluents also dictate increasingly lower P discharge limits. In the Unites States, National Pollution Discharge Elimination System (NPDES) permits often specify values ranging from 0.1 to 0.5 mg-P/L.(4) However, water resource recovery facilities (WRRFs) can struggle to meet increasingly lower regulations using existing P removal processes.(4−6)

Adsorption technologies offer strong potential for achieving very low concentrations of inorganic phosphate (P_i), ranging from 0.01 to 0.1 mg-TP/L, in scenarios of high water/wastewater volume and relatively low P_i concentrations such as in WRRF effluents or in lakes or reservoirs.(7−9) A wide variety of P_i adsorbents (some of which are reversible, which facilitates P_i recovery) have been evaluated, ranging from waste materials (biochar, slag, etc.) to metal oxide-based engineered adsorbents. Metal oxide-based P_i adsorbents (e.g.,

featuring lanthanum, iron, copper, magnesium, and/or zirconium) offer an effective approach to achieving ultralow P_i removal requirements and some offer P_i recovery for subsequent reuse.(9)

Phosphate-binding proteins (PBP) have recently attracted attention as alternative adsorbents capable of ultralow P_i removal.(10−14) The *PstS* PBP is the P_i-binding subunit of the P_i-specific transporter (Pst) system in bacteria. The Pst system is specifically evolved to import P_i when P_i is present at low levels, which demands ultraselective and high-affinity P_i binding and transport.(15,16) Removal of P_i to ultralow concentrations has been demonstrated using PBP expressed in bacterial cells' periplasmic space, expressed on the cells' surface, or immobilized on Sepharose beads.(10−12,14,17,18) Beyond P_i removal, Venkiteshwaran et al. (2018)(14) investigated pH and temperature conditions to induce controlled P_i desorption from immobilized PBP. They demonstrated that high pH conditions (pH 12.5) released >90% of P_i adsorbed on immobilized PBP. Additionally, the PBP maintained its initial activity for a minimum of 10 P_i adsorption and desorption cycles. This demonstration of PBP's reuse as an adsorbent able to remove and recover P_i further evidence its potential as an alternative to metal oxide-based ion exchangers.

Kumar et al. (2019)(9) suggested categorizing the costs of P_i adsorption technologies as (1) adsorbent production; (2) adsorbent regeneration and reusability; and (3) operation under practical parameters related to adsorption kinetics, affinity, selectivity, and the adsorbent's operational pH and temperature ranges. Newly developed P_i adsorbents, e.g., PBP-based, should be characterized accordingly for more complete evaluation and comparison against existing adsorbents. Therefore, the objective of this study was to investigate the adsorption kinetics, affinity, thermodynamics, and selectivity, as well as the effect of pH and temperature on P_i adsorption using immobilized PBP systems. Parameters were estimated using conventional adsorption models, and the results were compared with existing metal oxide-based P_i adsorbents.

2. Materials and Methods

2.1. Expression and Purification of PBP

The PBP used in this study was a His-tagged single-cysteine mutant variant (A197C) of the mature *E. coli* PBP developed as a phosphate biosensor.(20) The *pstS* gene plasmid (#78198, Addgene, Cambridge, MA) was transformed into BL21(DE3) *E. coli* competent cells. The cells were then cultured for protein expression in accordance with Venkiteshwaran et al.'s (2018)(14) protocol. After induction, the culture was centrifuged and the pellets were resuspended in 100 mL of buffer containing 10 mM Tris-HCl and 1 mM $MgCl_2$ (hereon, reaction buffer) at pH 8.0, and the mixture was sonicated 4 times for 30 s at 200 W with a 5 s on/off pulse cycle. The lysate was collected following centrifugation at 6000g for 45 min and passed through a 25 mL_{BV} (settled bead volume, where BV = bed volume) Ni Sepharose Fast Flow resin column (GE Healthcare Bio-Sciences, Pittsburgh, PA. The protein was eluted using 20 mM Na_3PO_4, 0.5 M NaCl, 0.5 M imidazole, pH 7.4 buffer, as specified by the manufacturer. The presence of the protein in the eluted fractions was verified using SDS-PAGE. Fractions containing PBP were pooled and concentrated using a 10 kDa cutoff spin concentrator (Vivaspin 20, GE Healthcare Bio-Sciences). The concentration of the purified PBP was 92 ± 6 mM, as quantified using the Quick Start Bradford Protein Assay (Bio-Rad Laboratories Inc., Hercules, CA), using bovine serum albumin as a standard (ThermoFisher Scientific, Waltham, MA). The purified PBP was aliquoted, frozen using liquid nitrogen, and stored at −80 °C until further use.

2.2. PBP Immobilization

In order to preserve the activity of the purified PBP at −80 °C, PBP immobilization was conducted in small batches at four different times using different volumes of purified PBP and NHS beads according to experimental needs. The detailed PBP immobilization protocol is described by Venkiteshwaran et al. (2018).(14) After dialyzing and immobilizing the purified PBP on 45–165 µm diameter NHS-activated Sepharose 4 Fast Flow beads (GE Healthcare Bio-Sciences), the resulting coupling density was 73–88 nmol-PBP/mL_{BV}-NHS beads. This provided a

theoretical P_i adsorption capacity of 73–88 nmol-P_i/mL_{BV}-NHS beads since 1 mol PBP can adsorb 1 mol P_i.(21,29,33) This coupling density was much lower than the maximum 16–23 μmol-protein/mL-NHS beads reported by the bead manufacturer. Although suboptimal, this coupling density was sufficient to complete the study objectives. Increased coupling densities could be achieved by purifying much larger batches of PBP in future applications.

The majority of the legacy P_i already adsorbed on the PBP during expression and purification was removed by washing the PBP-bound NHS beads (hereon, PBP resin) with 5_{BV} of reaction buffer at pH 12.5. This desorption method was the top performing approach tested by Venkiteshwaran et al. (2018),(14) with ∼90% legacy P_i desorption from the PBP resin. The PBP resins were kept at 4 °C and used within 48 h. A control set of resin was prepared following the same procedure used for the PBP resin, except with no addition of PBP.

2.3. Kinetics of Pi Adsorption by PBP resin

Triplicate P_i adsorption kinetics experiments were conducted in batch tests in 100 mL Econo-Columns (Bio-Rad Laboratories Inc.) containing 3 mL_{BV} PBP resin. An initial volume of 100 mL of reaction buffer at pH 7.1, 22 °C containing 10 μM P_i (1000 nmol P_i) was added to ensure P_i saturation of the PBP beads (the theoretical capacity of the PBP beads was 80 nmol-P_i/mL_{BV}). Immediately after the addition of the reaction buffer, the column was closed and mixed at 30 rpm on a Roto-Torque Variable Speed end-over-end rotator. Samples were collected after 0.5, 1, 2, 5, 10, 15, 30, and 60 min. The 1 mL samples were analyzed for P_i using the ascorbic acid method.(21) NHS resin with no PBP (control resin) was tested in parallel to evaluate potential P_i adsorption on the NHS resin itself.

2.4. Effect of pH and Temperature on Pi Adsorption Using PBP Resin

The effects of pH and temperature on P_i adsorption using PBP resin were tested in batch tests in 10 mL Econo-Columns containing 0.1 mL_{BV} PBP resin. The pH experiments were conducted at a constant temperature of 22 °C and at 4 different pH conditions (3.2, 5.1, 7.1, and 9.3) by adjusting the pH of the reaction buffer using 1 M HCl or 1 M NaOH. The theoretical capacity of the PBP resin in the pH experiment was 73 nmol-P_i/mL_{BV}.

The temperature experiments were conducted at a constant pH of 7.1 and 4 different temperatures: 14, 22, 37, or 43 °C. The 10 mL column containing 0.1 mL_{BV} PBP resin and the reaction buffer were preheated to the desired temperature for 30 min before initiating the experiment. The theoretical capacity of the PBP resin in the temperature experiment was 78 nmol/mL_{BV}.

For each condition, triplicate sets of PBP resins were exposed to 10 mL reaction buffer containing 9 different P_i concentrations: 0.15, 0.25, 0.5, 0.75, 1, 1.25, 1.5, 1.75, or 2 μM P_i. Immediately after adding the reaction buffer, the columns in both pH and temperature experiments were closed and mixed at 30 rpm on a Roto-Torque Variable Speed end-over-end rotator for 60 min. The reaction buffer was then collected and analyzed for P_i. A similar test using control resin was conducted in parallel.

2.5. Effect of Anion Concentration on Pi Adsorption by PBP Resin

P_i adsorption by PBP resin was analyzed at 3 different concentrations of anion mixtures containing Br^-, NO_2^-, NO_3^-, SO_4^{2-}, and HCO_3^- (dosed using the respective salt: NaBr, $NaNO_2$, $NaNO_3$, Na_2SO_4, and $NaHCO_3$). These mixtures represent common water/wastewater anions and variations in their concentrations in most surface water and treated wastewater effluent.(22,23) No Cl^- was added as the reaction buffer (10 mM Tris-HCl, 1 mM $MgCl_2$ at pH 7.1) itself contained approximately 530 mg/L Cl^- due to the presence of $MgCl_2$ and addition 1 M HCl to adjust the reaction buffer pH. The control set was analyzed using the reaction buffer with no added anions. The high anion concentration reaction buffer contained 6 mg/L Br^-, 6 mg/L NO_2^-, 4 mg/L NO_3^-, 102 ± 3 mg/L SO_4^{2-}, and 120 mg/L HCO_3^-. The low anion concentration reaction buffer was prepared by diluting the high anion concentration reaction buffer by half using reaction buffer with no added anions. The pH of the low and high

anion reaction buffer was readjusted to 7.1. The concentrations of Cl^-, NO_2^-, NO_3^-, and SO_4^{2-} were confirmed using a DIONEX ICS-110 Ion Chromatograph (ThermoFisher Scientific), and the concentration of Br^- and HCO_3^- was based on the added amount.

The experiments were conducted in triplicate batch tests in 10 mL Econo-Columns containing 0.1 mL_{BV} PBP resin at constant temperature and pH (22 °C, pH 7.1). At each anion concentration, triplicate sets of PBP resins were exposed to 10 mL reaction buffer containing 9 different P_i concentrations (0.15, 0.25, 0.5, 0.75, 1, 1.25, 1.5, 1.75, or 2 μM P_i). After the addition of the reaction buffer, the columns were closed and mixed at 30 rpm on a Roto-Torque Variable Speed end-over-end rotator for 60 min. The reaction buffer was then collected and analyzed for P_i. A parallel set of control resin tests was performed. The theoretical capacity of the PBP beads in these experiments was 88 nmol-P_i/mL_{BV}.

2.6. Modeling Adsorption Kinetics

Pseudo first order (PFO) and pseudo second order (PSO) models are widely used to describe the rate of adsorption in batch systems.(24)

2.6.1. Pseudo First Order Expression

The PFO reaction model is shown in eq 1.(24) (The linearized form of the model is shown in the Supporting Information (SI)).

$$q_t = q_e(1 - e^{-k_{PFO}t})$$

(1)

where q_e and q_t are the amounts of P_i adsorption (nmol) per mass of PBP (nmol) at equilibrium and at any time t (min), respectively, and k_{PFO} (min^{-1}) is the PFO rate constant.

The adsorption capacity at time t (q_t) and equilibrium (q_e) was calculated using eq 2

$$q_i = \frac{(C_0 - C_i) \times V}{M}$$

(2)

where C_0 is the initial P_i concentration (nM) in the solution; C_i represents C_e or C_t, which are the P_i concentrations (nM) at equilibrium or time t (min), respectively; V is the volume of solution (L); and M is the mass of PBP (nmol).

2.6.2. Pseudo Second Order Expression

The PSO adsorption model is shown in eq 3.(25) (The linearized form of the model is shown in the SI).

$$q_t = \frac{q_e^2 \times k_{PSO} \times t}{q_e \times k_{PSO} \times t + 1}$$

(3)

where q_e and q_t are the amount of P_i adsorbed at equilibrium and at any time t (min), respectively (nmol-P_i/nmol-PBP), and k_{PSO} is the PSO rate constant (nmol-PBP/nmol-P_i-min).

2.7. Modeling Adsorption Isotherms

Adsorption isotherms were modeled using Langmuir (eq 4) and Freundlich (eq 6) isotherms.(26,27) (The linearized forms of the models are shown in the SI).

$$q_e = \frac{q_{\max} K_L C_e}{(1 + K_L C_e)}$$

(4)

where q_{max} is the maximum adsorption capacity (nmol-P_i/nmol-PBP), q_e is the adsorption capacity at equilibrium (nmol-P_i/nmol-PBP), C_e is the P_i concentration remaining in the solution at equilibrium (μM), and K_L is the Langmuir constant (μM^{-1}).

The Langmuir constant, K_L, indicates the affinity between an adsorbent and adsorbate. It is used to describe affinity in most adsorption studies and can also be related to the biochemical parameters primarily used to describe protein–ligand binding mechanisms in literature (eq 5).(28)

$$K_L = K_B = \frac{1}{k_D}$$

(5)

where K_B is protein–ligand binding affinity (μM^{-1}) and k_D is the protein–ligand dissociation constant (μM), which describes the concentration of the ligand in the solution when half of the protein adsorption sites are occupied by the ligand.

Previous studies of *PstS* PBP have described its affinity for P_i in terms of k_D.(20,29) Therefore, eq 5 establishes a relationship between the estimated Langmuir constant from this study with previously determined k_D values for PBP-P_i binding. The k_D values for *PstS* PBP range from 0.03 to 0.1 μM(20,29) or 10 to 33 μM^{-1} (105 to 347 L/mg P_i) in terms of the Langmuir constant (K_L).

The Freundlich isotherm model is shown in eq 6

$$q_e = K_F \times C_e^{1/n}$$

(6)

where K_F is the Freundlich coefficient (nmol-P_i/nmol-PBP) and n is a dimensionless empirical constant.

2.8. Thermodynamics of Adsorption

Thermodynamics, like isotherms, play an essential role in characterizing adsorption equilibrium and mechanisms.(30) Important thermodynamic parameters for adsorption include the change in enthalpy, the change in entropy, and the change in standard binding or Gibb's free energy (eq 7),(28)

$$\Delta G = \Delta H - T \times \Delta S$$

(7)

where ΔH is the change in enthalpy (kJ/mol), ΔS is the change in entropy (kJ/mol-K), ΔG is the binding or Gibb's free energy (kJ/mol), and T is temperature (K).

The binding or Gibb's free energy can be related to the binding constant K_B of a protein–ligand interaction, as shown in eq 8,(28)

$$\Delta G = -R \times T \times \ln(K_B)$$

(8)

where R is the universal gas constant (8.314×10^{-3} kJ/mol-K), T is temperature (K), and K_B is the binding constant (M^{-1}). Using eq 5, the binding constant (K_B) can be substituted with the Langmuir constant (K_L) to determine the binding energy (ΔG).

With a combination of eqs 7 and 8, the change in enthalpy (ΔH) and the change in entropy (ΔS) can be determined by plotting $\ln(K_L)$ vs 1/T (eq 9)

$$\ln(K_L) = -\frac{\Delta H}{R \times T} + \frac{\Delta S}{R}$$

(9)

2.9. Analytical Methods and Statistical Analysis

All PBP resin P_i concentration data was normalized to the corresponding control test. The normalized data was also compared to the theoretical P_i adsorption capacity of the PBP resin to calculate the fraction of P_i adsorbed. The ascorbic acid method was used to quantify P_i using a HACH DR 3900 spectrophotometer with 2.5 cm light path.(21) The minimum detection limit (MDL) was 0.09 μM P_i, as determined using USEPA (2016)(31) methods. Only data for which $C_e \geq$ MDL were used to fit in the Langmuir and Freundlich isotherm models.

To facilitate comparisons against other adsorbents using comparable units, we converted values from molar to mass-based units (1 mol P_i = 94.97 g P_i). The adsorption capacity (q) was converted to units of mg-P_i/g-PBP resin, PSO rate constant (k_{PSO}) to units of g-PBP resin/mg-P_i-min, and Freundlich coefficient (K_F) to units of mg-P_i/g-PBP resin. An assumed resin density of 1 g/mL was used together with each experiment-specific protein coupling density (nmol-PBP/mL_{BV}) in the calculations.

The statistical differences in adsorption capacity and P_i affinity at different conditions were determined using one-way ANOVA with Tukey post hoc analysis using GraphPad Prism 6 (GraphPad Software, Inc., La Jolla, CA). Langmuir and Freundlich isotherm modeling were conducted using Microsoft Excel 2016 (Version 16) with the added statistical software package XLStat Pro 2014 (Addinsoft). All statistics were performed at a significance level $\alpha = 0.05$.

3. Results and Discussion

3.1. Kinetics of Pi Adsorption: PBP Resin Offers the Fastest Rate of Adsorption among Known Adsorbents

Phosphate adsorption kinetics using PBP resin are shown in Figure 1. The PBP resin attained its maximum P_i adsorption capacity within 0.5 min of introducing the P_i solution (which was the fastest sample we were able to process), and no further statistical change in adsorption capacity was observed for 60 min. The average adsorption capacity of the PBP resin between 0.5 and 60 min was 0.85 ± 0.02 nmol-P_i/nmol-PBP ($6.5 \times 10^{-3} \pm 1.5 \times 10^{-4}$ mg-P_i/g-PBP resin) or 85 ± 2% of the theoretical maximum capacity. Similarly, Venkiteshwaran et al. (2018)(14) observed a maximum P_i adsorption of 83–88% of the theoretical capacity of the PBP resin. Possible reasons for observed capacities being less than the theoretical 100% could be incomplete desorption of legacy P_i and/or denaturation of PBP during the purification and immobilization process.(14)

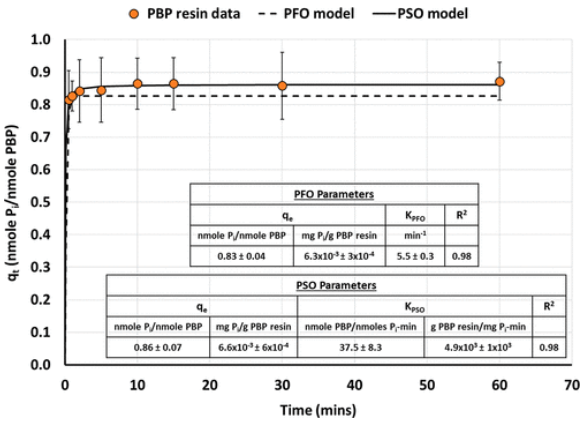

Figure 1. Adsorption kinetics of PBP resin fitted with pseudo first order (PFO) and pseudo second order (PSO) models. The vertical error bars represent the standard deviation of triplicate analyses. The PBP resin attained its maximum P_i adsorption capacity within 0.5 min with no further statistical change thereafter. Nonlinear forms of both PFO and PSO models showed a good fit with similarly high correlation coefficients of $R^2 = 0.98$.

The nonlinear forms of both PFO and PSO models showed strong fits with the experimental data, with $R^2 = 0.98$ (Figure 1). Once linearized, however, the PSO model provided the best fit with $R^2 = 0.99$ (Figure S1B), whereas $R^2 = 0.51$ for the linearized PFO model (Figure S1A). The PSO adsorption kinetics model is commonly used in a wide range of adsorbent studies, including studies investigating reversible P_i adsorbents such as ion exchange resins.(19,32) Using the estimated PSO model parameters (k_{PSO} and q_e), the time required to attain 95% of equilibrium adsorption capacity ($t_{95\%}$) of the PBP resin was calculated as 0.64 ± 0.2 min. This is the shortest $t_{95\%}$ observed among the 25 P_i adsorbents surveyed from previous studies within the last 6 years (Table S1).

3.2. Adsorption Isotherm Modeling: Langmuir Models Provide the Best Fit for PBP Resin

Langmuir and Freundlich isotherm models are most commonly applied to fit adsorption processes.(26)Figure 2 shows an adsorption isotherm of PBP resin tested at 22 °C and pH 7.1 fitted using Langmuir and Freundlich isotherms. The nonlinear Langmuir model provided a better fit ($R^2 = 0.92$) than the nonlinear Freundlich model ($R^2 = 0.84$). In the linearized form, Langmuir also provided a better fit than Freundlich ($R^2 = 0.99$ versus $R^2 = 0.82$, respectively, Figure S2). This finding agrees with the mechanism of protein–ligand binding in PBP and other adenosine triphosphate-binding cassette (ABC) type transporter proteins.(15,33) Specifically, one PBP is expected to bind one P_i molecule. The basic Langmuir model assumption is that adsorption occurs in a monolayer on the surface of the adsorbent, indicating that only one ligand molecule could be adsorbed on one adsorption site and intermolecular forces decrease with distance. It also assumes that the adsorbent surface is homogeneous in character and has identical and energetically equivalent adsorption sites.(26)

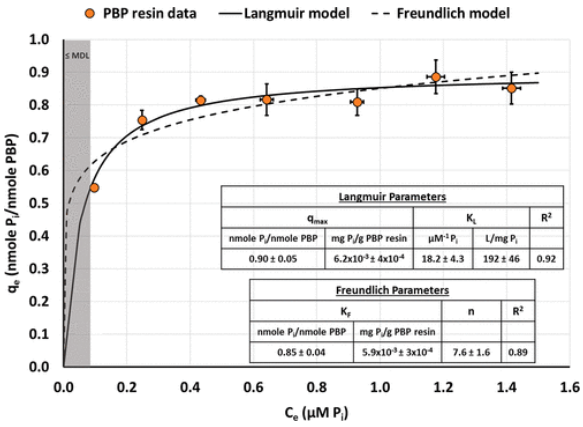

Figure 2. Adsorption isotherms of PBP resin (22 °C and pH 7.1) showing Langmuir and Freundlich isotherm model fits. The vertical and horizontal error bars represent the standard deviation of triplicate analyses. The minimum detection limit (MDL) of P_i analysis was 0.09 µM. Only q_e and C_e values corresponding to $C_e \geq$ MDL are shown in the plot and used to fit the Langmuir and Freundlich models. On the basis of the estimated correlation coefficients, the Langmuir isotherm model ($R^2 = 0.92$) provided a better fit for the experimental data than the Freundlich model ($R^2 = 0.84$). This was expected as one active site on PBP can adsorb only one molecule of P_i.

The maximum adsorption capacity (q_{max}) from the Langmuir equation was estimated as 0.90 ± 0.05 nmol-P_i/nmol-PBP ($6.2 \times 10^{-3} \pm 4 \times 10^{-4}$ mg-P_i/g-PBP resin), which is 90 ± 5% of the theoretical maximum capacity and is statistically similar to the adsorption capacity observed in the kinetic experiment. The Langmuir isotherm constant (K_L), which describes the affinity of the PBP resin for P_i, was estimated as 18.2 ± 4.3 μM^{-1} P_i (192 ± 46 L/mg-P_i). The observed K_L value of the PBP resin was within the expected range of 10–33 μM^{-1} P_i, as calculated from previously estimated dissociation constants (k_D = 0.03–0.1 µM) for suspended PBP.(20,29) This indicates that immobilization does not affect PBP affinity for P_i. The estimated K_L value of the PBP resin was 15 to 10^4 times higher than other surveyed P_i adsorbents (Table S1**)**.

3.3. Effect of pH on Pi Adsorption: PBP Resin's Adsorption Decreases at Low and High pH

The adsorption isotherms for PBP resin at constant temperature (22 °C) and variable pH are shown in Figure 3. The curves were fit using the Langmuir isotherm model. In comparison to the control condition at pH 7.1, the maximum adsorption capacities were statistically similar at pH 3.2, 5.1, and 9.3 (p = 0.96). There was no significant difference between the PBP resin adsorption affinity at pH 5.1 and the control condition at pH 7.1 (p > 0.05). However, the PBP resin's P_i affinity dropped significantly at pH 3.2 (75 ± 6.4%, p = 0.01) and pH 9.3 (54 ± 8.6%, p < 0.04) compared to the control condition.

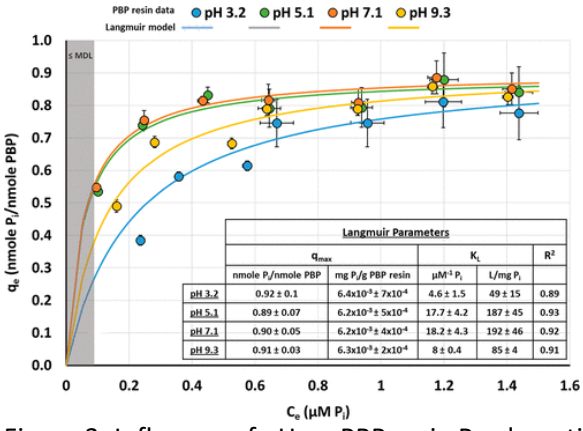

Langmuir Parameters

	q_{max}		K_L		R^2
	nmole P_i/nmole PBP	mg P_i/g PBP resin	μM^{-1} P_i	L/mg P_i	
pH 3.2	0.92 ± 0.1	$6.4x10^{-3}$ ± $7x10^{-4}$	4.6 ± 1.5	49 ± 15	0.89
pH 5.1	0.89 ± 0.07	$6.2x10^{-3}$ ± $5x10^{-4}$	17.7 ± 4.2	187 ± 45	0.93
pH 7.1	0.90 ± 0.05	$6.2x10^{-3}$ ± $4x10^{-4}$	18.2 ± 4.3	192 ± 46	0.92
pH 9.3	0.91 ± 0.03	$6.3x10^{-3}$ ± $2x10^{-4}$	8 ± 0.4	85 ± 4	0.91

Figure 3. Influence of pH on PBP resin P_i adsorption at constant temperature (22 °C). The data was fit using the Langmuir isotherm model. The vertical and horizontal error bars represent the standard deviation of triplicate analyses. The minimum detection limit (MDL) of P_i analysis was 0.09 µM. Only q_e and C_e values corresponding to C_e values ≥ MDL are shown in the plot and used to fit the Langmuir model. The maximum adsorption capacities (q_{max}) were statistically similar at all pH conditions tested (p = 0.96). There was no statistical difference (p > 0.05) between the PBP resin's estimated Langmuir constant (K_L) at pH 5.1 and pH 7.1. In contrast, the PBP resin's P_i affinity was significantly reduced at pH 3.2 and pH 9.3 (75 ± 6.4% and 54 ± 8.6%, respectively), as compared to the control condition (p < 0.05).

Venkiteshwaran et al. (2018)(14) also observed that increasing the pH above 9 reduced PBP resin's P_i affinity, inducing P_i desorption, with near-complete desorption occurring at pH ≥ 12.5. There was no loss of PBP structural integrity at pH > 9, and it was postulated that the decrease in PBP-P_i adsorption at pH > 9 may be due to deprotonation of 7 different amino acid residues that interact with P_i in the active site, with pK_a values range

from 9.04 to 9.6.(14) Another possible explanation for desorption at pH > 9 is the deprotonation of P_i ions in the water at high pH. P_i can exist as H_3PO_4, $H_2PO_4^-$, HPO_4^{2-}, or PO_4^{3-} depending on solution pH (pK_a values of 2.15, 7.2, and 12.35, Figure S3).(34) Luecke and Quiocho (1990)(15) studied the atomic features of PBP using X-ray crystallography and found that PBP had a strong affinity for the monobasic ($H_2PO_4^-$) and dibasic (HPO_4^{2-}) forms of P_i, with a slight preference for the latter. They reported that the presence of two protons on the third and fourth oxygen atoms in $H_2PO_4^-$ or single proton on the fourth oxygen atom in HPO_4^{2-} is critical for P_i binding to PBP.(15) There is no information on PBP binding fully deprotonated P_i (PO_4^{3-}) at high pH. Accordingly, we postulate that the low binding affinity at pH > 9 could be due to deprotonation of amino acid residues in the active site as well as P_i deprotonating from the HPO_4^{2-} form to the PO_4^{3-} form, with lowest P_i binding observed at pH ≥ 12.5 when PO_4^{3-} dominates (pK_{a3} = 12.35).(14) On the basis of available literature, it is presently not clear whether deprotonation of P_i or the amino acid residues is the dominant factor inducing P_i adsorption from PBP at pH > 9.

There are also no studies of PBP-P_i binding at pH < 4.5. Unlike at pH ≥ 9, deprotonation of the active site amino acid residues will not play a role as the amino acids will maintain a positive charge at pH 3.2. Denaturation of PBP was also eliminated as a possibility. This was tested using a batch of PBP resin exposed to pH 3.2 for 30 min, washed with 3 bed volumes of reaction buffer at pH 7, and exposed to P_i for 30 min. The results showed no difference in its adsorption capacity or affinity compared to P_i adsorption to PBP resin under control conditions. At low pH (≤3.2), the form of P_i in the water may be the dominant factor in reduced PBP-P_i affinity. As the pH decreases below pH 4.5, P_i shifts from monobasic $H_2PO_4^-$ to the fully protonated H_3PO_4 form (pK_{a1} = 2.15) (Figure S3). The protonation of the second, third, and fourth oxygen atoms will completely eliminate columbic interaction between the neutral P_i and the positively charged amino acid residues in the PBP active site. Accordingly, the ideal pH range for high-affinity P_i adsorption using PBP resin would be between pH 4.5 and pH 9, which is below the pK_a of the amino acids in the active site and in the pH range where the partially protonated $H_2PO_4^-$ and HPO_4^{2-} forms dominate.

3.4. Effect of Temperature and the Thermodynamic Parameters of Adsorption: Pi Adsorption Using PBP Resin Is Thermodynamically Favorable and Spontaneous

The adsorption isotherms for PBP resin at different temperatures (14, 22, 37, and 43 °C) and constant pH (7.1), along with the estimated Langmuir isotherm parameters, are shown in Figure 4. There was no statistical difference in the estimated maximum P_i adsorption capacity or adsorption affinity across the temperature range 14–37 °C tested (p = 0.22). However, increasing the temperature to 43 °C reduced P_i adsorption affinity by 32 ± 8% compared to the control condition at 22 °C (p = 0.02).

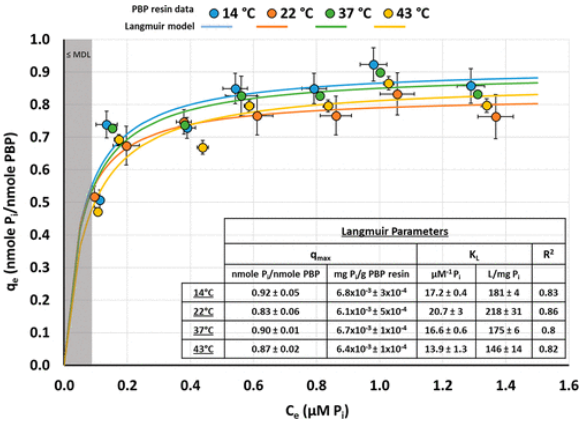

Langmuir Parameters	q_{max}		K_L		R^2
	nmole P_i/nmole PBP	mg P_i/g PBP resin	µM^{-1} P_i	L/mg P_i	
14°C	0.92 ± 0.05	6.8x10^{-3} ± 3x10^{-4}	17.2 ± 0.4	181 ± 4	0.83
22°C	0.83 ± 0.06	6.1x10^{-3} ± 5x10^{-4}	20.7 ± 3	218 ± 31	0.86
37°C	0.90 ± 0.01	6.7x10^{-3} ± 1x10^{-4}	16.6 ± 0.6	175 ± 6	0.8
43°C	0.87 ± 0.02	6.4x10^{-3} ± 1x10^{-4}	13.9 ± 1.3	146 ± 14	0.82

Figure 4. Adsorption isotherm of PBP resin at different temperatures and constant pH (7.1), along with the estimated Langmuir isotherm parameters. The vertical and horizontal error bars represent the standard deviation of triplicate analyses. The minimum detection limit (MDL) of P_i analysis was 0.09 µM. Only q_e and

C_e values corresponding to C_e values ≥ MDL are shown in the plot and used to fit the Langmuir model. The maximum adsorption capacity (q_{max}) was statistically similar at all temperatures tested ($p > 0.05$). The estimated Langmuir constant (K_L) was statistically similar between 14 to 37 °C. However, the K_L at 43 °C was 32 ± 8% less than the control conditions at 22 °C ($p = 0.02$).

A plot of ln(K_L) against 1/T was used to determine the thermodynamic fitting parameters of P_i adsorption on PBP resin (Figure S4). For a ligand-protein binding process, Δ*H*, or the binding enthalpy, reflects the energy change of the system when the ligand binds to the protein. The net entropy change, Δ*S*, indicates the change in degrees of freedom associated with the ligand-protein binding process. Together, Δ*S* and Δ*H* determine the overall sign and magnitude of the binding free energy (Δ*G*); therefore, Δ*H* and Δ*S* are considered the driving factors for protein–ligand binding. Only when the change in binding free energy is negative can protein–ligand binding occur spontaneously and the magnitude of the difference in free energy (Δ*G*, i.e., the extent of the negative free energy change upon binding) determines the stability of the protein–ligand complex.

The estimated Δ*H* value was −6.3 ± 1.3 kJ/mol, indicating that adsorption was exothermic. Values of Δ*H* < 80 kJ/mol indicate that noncovalent interactions such as van der Waals forces, hydrogen bonds, ionic pairs, and other polar and nonpolar interactions play an important role during the adsorption process.(28) The estimated Δ*S* value for P_i-PBP resin adsorption was 0.12 ± 0.004 kJ/mol-K, suggesting a marginal gain in entropy as a result of P_i-PBP resin binding. The positive Δ*S* along with negative Δ*H* contributed favorably to the overall binding free energy (Δ*G*). The estimated Δ*G* values were negative (Δ*G* = −39.7 ± 0.1 to −43.2 ± 0.2 kJ/mol), indicating that the adsorption process was spontaneous at all temperatures tested in this study. The spontaneity of the binding reaction increased significantly as temperature increased from 14 to 37 °C ($p < 0.001$); however, no statistical difference was observed between 37 and 43 °C (p = 0.49).

3.5. Selectivity of Pi Adsorption by PBP Resin: Common Anions Do Not Impede Adsorption

The influence of low and high anion concentrations on PBP resin P_i adsorption at constant temperature and pH (22 °C, pH 7.1) along with the estimated Langmuir isotherm parameters is shown in Figure 5. The Cl^- concentration in the reaction buffer was initially high (≈530 mg/L) due to the addition of 1 N HCl to bring the buffer pH to 7.1. Therefore, the presence of high Cl^- ions did not affect the P_i-PBP resin adsorption process based on the range of experiments conducted using the reaction buffer in this study. In comparison to the control condition (no added anions), the presence of other common water/wastewater anions (Br^-, NO_2^-, NO_3^-, SO_4^{2-}, and HCO_3^-) at low and high anionic concentrations did not significantly influence the PBP resin's adsorption capacity ($p = 0.22$) or P_i affinity ($p = 0.33$). These results confirm that the PBP resin can maintain its P_i adsorption capacity, affinity, and selectivity in the presence of high anion concentrations, thereby supporting its potential as a P_i adsorbent in real water or wastewater applications. Beyond anions, organic material can also affect P_i adsorption; accordingly, further assessment of PBP resin performance in more complex matrices, specifically in real water and wastewater, is needed in future studies.

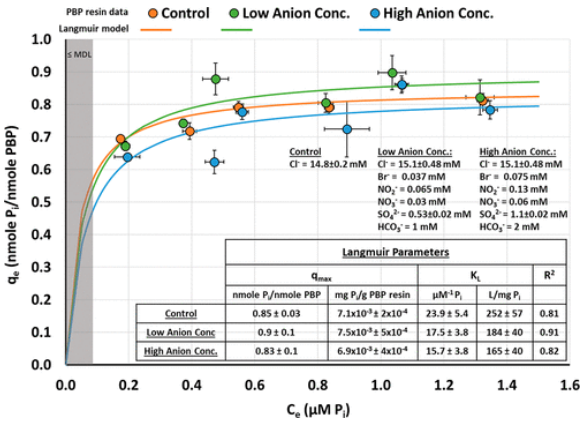

Figure 5. Influence of low and high anion concentration on PBP resin P_i adsorption at constant temperature and pH (22 °C, pH 7.1), along with the estimated Langmuir isotherm parameters. The vertical and horizontal error bars represent the standard deviation of triplicate analyses. Only q_e and C_e values corresponding to C_e values ≥ MDL of 0.09 µM are shown in the plot and used to fit the Langmuir model. The maximum adsorption capacity (q_{max}) and Langmuir constant (K_L) were statistically similar at all anion concentrations tested ($p > 0.05$).

3.6. Comparison of PBP Resin against Other Adsorbents

The results of our analysis of PBP resin's adsorption kinetics, affinity, thermodynamics, response to temperature and pH, and selectivity were compared with 25 recently described reversible adsorbents from a survey of 21 reports published within the last 6 years (Figure 6, Table S1). The 25 adsorbents varied in the type of metal oxides used, e.g., lanthanum, iron, copper, magnesium, zirconium, or combinations thereof as well as in their base material composition, e.g., metal chelating polymers, granular activated carbon, hydrogel, or biochar. All surveyed adsorbents were also characterized using the Langmuir isotherm model to facilitate direct comparisons of adsorption parameters of the PBP resin and the other adsorbents.

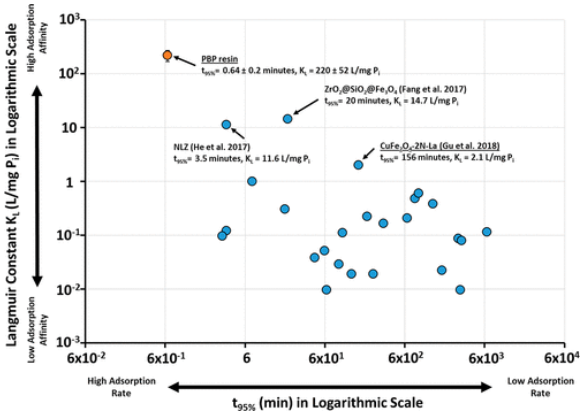

Figure 6. Comparison of PBP resin's P_i affinity, or Langmuir constant (K_L), and rate of adsorption (represented by the time to achieve 95% of equilibrium capacity, $t_{95\%}$) with 25 different P_i adsorbents from literature. The vertical and horizontal error bars represent the standard deviation of triplicate analyses for this study. The PBP resin's P_i affinity and adsorption rate were substantially greater than the 25 other P_i adsorbents surveyed in recent literature (Table S1 lists all adsorbents analyzed along with the associated adsorption parameters).

As shown in Figure 6, the PBP resin outperformed the other adsorbents with respect to adsorption kinetics and affinity. The PBP resin took 0.64 ± 0.2 min to attain 95% of its equilibrium adsorption capacity ($t_{95\%}$), which was 5 to 10^4 times less than the range of other adsorbents surveyed. PBP resin's adsorption affinity (Langmuir isotherm constant, K_L) was 21 ± 5 μM^{-1} P_i (220 ± 52 L/mg P_i, averaged across all tests performed at 22 °C, pH

7.1), which was 15 to 10^4 times higher than the other adsorbents surveyed. The PBP resin demonstrated no change in adsorption affinity between pH 5.1 to 7.1, between temperatures 14 and 37 °C, and at high anion salt concentrations, which was comparable to most previously studied adsorbents.(19)

Furthermore, PBP resin can provide a distinctive advantage over existing P_i adsorbents through its ability to selectively adsorb P_i in the presence of arsenate ions.(35) Arsenate shares the same tetrahedral structure as P_i, and most metal oxide-based P_i adsorbents are unable to distinguish between the two oxyanions. Alternately, the PBP used in this study (*E. coli* A197C) offers 50–100 times higher P_i binding affinity for P_i compared to arsenate.(29) PBPs from other microorganisms such as *P. fluorescens*, *Halomonas* sp. GFAJ-1, and *K. variicola* are also able to discriminate P_i from arsenate, even when the arsenate concentration is 3000 to 4000-fold higher than the P_i concentration.(35) Arsenate was not included in this study as concentrations in most surface waters and domestic wastewaters are typically $\ll$10 μg/L (whereas phosphate and other common anions are present at mg/L levels); thus, arsenate offers limited competition in most surface waters and municipal wastewaters.(36) However, wastewater from mining and petrochemical industries and contaminated freshwater sources in some regions of the world can have high arsenate concentrations where an arsenate-discriminating P_i adsorbent would be beneficial.(36) PBP resins may offer an advantage in such settings, and arsenate competition should be investigated in the future.

As shown here, PBP systems offer exceptional affinity and kinetics of P_i adsorption, exceeding the performance of existing metal-based adsorbents by several fold. The PBP resin was not deleteriously impacted by typical ranges of temperature, pH, and anion concentrations. These characteristics are prerequisites for effective implementation in scenarios of high water/wastewater volume and relatively low P concentrations, e.g., to polish WRRF effluent prior to discharge or for remediation of P-sensitive lakes or reservoirs. The PBP resin has also demonstrated functionality as a reversible adsorbent by releasing P_i at pH ≥ 12.5, and maintaining performance for a minimum of 10 P_i adsorption/desorption cycles under controlled laboratory conditions.(14) This reversibility enables P_i recovery to support the circular phosphorus economy.

However, PBP systems are still in the very early stages of development. Future advances are needed to overcome significant limitations in order for PBP to be a cost-effective alternative to existing adsorbents. Specifically, the PBP resin's adsorption capacity depends on its protein coupling density, i.e., efficiency in immobilizing PBP onto a surface. On the basis of the P_i adsorption capacity (0.86 ± 0.07 nmol-P_i/nmol-PBP) and protein coupling density (73 to 88 nmol-PBP/mL_{BV}-PBP resin) measured in this study, the PBP resin's adsorption capacity ranged from 6×10^{-3} to 7.2×10^{-3} mg-P_i/g-PBP resin. Using the maximum protein coupling density of the resin (as reported by the manufacturer), the adsorption capacity of the PBP resin increases to 1.3 to 1.9 mg-P_i/g-PBP resin (Table S1). However, this maximum value is still an order of magnitude less than those of existing P_i adsorbents. Accordingly, future developments must focus on optimizing protein immobilization density to improve PBP resin's P_i adsorption capacity.

Additionally, PBP may be affected by the presence of organic matter, microorganisms, and proteolytic enzymes, which may hinder its viability in real water/wastewater conditions. Constituents in complex waters such as natural organic matter (e.g., humic acid) and multivalent cations (e.g., Ca^{2+}, Fe^{2+}/Fe^{3+}, Mg^{2+}) could also impede P_i adsorption by forming strong complexes with P_i, inhibiting its ability to bind to PBP.(37) Therefore, future investigations of the performance of PBP resin in actual water/wastewater matrices are essential in support of a more complete evaluation of the key factors governing the performance and economics of P_i removal and recovery using PBP resins.

Supporting Information

The Supporting Information is available free of charge at https://pubs.acs.org/doi/10.1021/acs.est.0c02272.

- Kinetics of P_i adsorption by PBP resin (linearized models), Langmuir and Freundlich adsorption isotherm modeling (linearized models), effect of pH on P_i speciation in water, thermodynamic parameters of adsorption, and Langmuir and pseudo second order kinetic model constants for 25 different adsorbents (PDF)

Terms & Conditions

References

1. Cordell, D.; Drangert, J.-O.; White, S. The Story of Phosphorus: Global Food Security and Food for Thought. *Glob. Environ. Chang.* **2009**, *19* (2), 292– 305, DOI: 10.1016/j.gloenvcha.2008.10.009
2. Dodds, W. K.; Bouska, W. W.; Eitzmann, J. L.; Pilger, T. J.; Pitts, K. L.; Riley, A. J.; Schloesser, J. T.; Thornbrugh, D. J. Eutrophication of U.S. Freshwaters: Analysis of Potential Economic Damages. *Environ. Sci. Technol.* **2009**, *43* (1), 12– 19, DOI: 10.1021/es801217q
3. USEPA Nutrient Criteria Technical Guidance Manuel. *United States Environ. Prot. Agency, Off. Water* **2000**, 197
4. USEPA Advanced Wastewater Treatment to Achieve Low Concentration of Phosphorus. *United States Environ. Prot. Agency, Off. Water Watersheds Reg.* **2007**, 73
5. Neethling, J. B.; Clark, D.; Pramanik, A.; Stensel, H. D.; Sandino, J.; Tsuchihashi, R. WERF Nutrient Challenge Investigates Limits of Nutrient Removal Technologies. *Water Sci. Technol.* **2010**, *61* (4), 945– 953, DOI: 10.2166/wst.2010.617
6. Gu, A. Z.; Liu, L.; Neethling, J. B.; Stensel, H. D.; Murthy, S. Treatability and Fate of Various Phosphorus Fractions in Different Wastewater Treatment Processes. *Water Sci. Technol.* **2011**, *63* (4), 804– 810, DOI: 10.2166/wst.2011.312
7. Sengupta, S.; Pandit, A. Selective Removal of Phosphorus from Wastewater Combined with Its Recovery as a Solid-Phase Fertilizer. *Water Res.* **2011**, *45* (11), 3318– 3330, DOI: 10.1016/j.watres.2011.03.044
8. Mayer, B. K.; Gerrity, D.; Rittmann, B. E.; Reisinger, D.; Brandt-Williams, S. Innovative Strategies to Achieve Low Total Phosphorus Concentrations in High Water Flows. *Crit. Rev. Environ. Sci. Technol.* **2013**, *43* (4), 409– 441, DOI: 10.1080/10643389.2011.604262
9. Kumar, P. S.; Korving, L.; van Loosdrecht, M. C. M.; Witkamp, G.-J. Adsorption as a Technology to Achieve Ultra-Low Concentrations of Phosphate: Research Gaps and Economic Analysis. *Water Res. X* **2019**, *4*, 100029, DOI: 10.1016/j.wroa.2019.100029
10. Choi, S. S.; Lee, H. M.; Ha, J. H.; Kang, D. G.; Kim, C. S.; Seo, J. H.; Cha, H. J. Biological Removal of Phosphate at Low Concentrations Using Recombinant Escherichia Coli Expressing Phosphate-Binding Protein in Periplasmic Space. *Appl. Biochem. Biotechnol.* **2013**, *171* (5), 1170– 1177, DOI: 10.1007/s12010-013-0187-1
11. Li, Q.; Yu, Z.; Shao, X.; He, J.; Li, L. Improved Phosphate Biosorption by Bacterial Surface Display of Phosphate-Binding Protein Utilizing Ice Nucleation Protein. *FEMS Microbiol. Lett.* **2009**, *299* (1), 44– 52, DOI: 10.1111/j.1574-6968.2009.01724.x
12. Yang, Y.; Ballent, W.; Mayer, B. K. High-Affinity Phosphate-Binding Protein (PBP) for Phosphorous Recovery: Proof of Concept Using Recombinant Escherichia Coli. *FEMS Microbiol. Lett.* **2016**, *363* (20), fnw240, DOI: 10.1093/femsle/fnw240

13. Yang, Y.; Shi, X.; Ballent, W.; Mayer, B. K. Biological Phosphorus Recovery: Review of Current Progress and Future Needs. *Water Environ. Res.* **2017**, *89* (12), 2122– 2135, DOI: 10.2175/106143017X15054988926424
14. Venkiteshwaran, K.; Pokhrel, N.; Hussein, F.; Antony, E.; Mayer, B. K. Phosphate Removal and Recovery Using Immobilized Phosphate Binding Proteins. *Water Res. X* **2018**, *1*, 100003, DOI: 10.1016/j.wroa.2018.09.003
15. Luecke, H.; Quiocho, F. A. High Specificity of a Phosphate Transport Protein Determined by Hydrogen Bonds. *Nature* **1990**, *347* (6291), 402– 406, DOI: 10.1038/347402a0
16. Blank, L. M. The Cell and P: From Cellular Function to Biotechnological Application. *Curr. Opin. Biotechnol.* **2012**, *23* (6), 846– 851, DOI: 10.1016/j.copbio.2012.08.002
17. Kuroda, A.; Kunimoto, H.; Morohoshi, T.; Ikeda, T.; Kato, J.; Takiguchi, N.; Miya, A.; Ohtake, H. Evaluation of Phosphate Removal from Water by Immobilized Phosphate-Binding Protein PstS. *J. Biosci. Bioeng.* **2000**, *90* (6), 688– 690, DOI: 10.1016/S1389-1723(00)90020-3
18. Hussein, F. B.; Venkiteshwaran, K.; Mayer, B. K. Cell Surface-Expression of the Phosphate-Binding Protein PstS: System Development, Characterization, and Evaluation for Phosphorus Removal and Recovery. *J. Environ. Sci.* **2020**, *92*, 129– 140, DOI: 10.1016/j.jes.2020.02.016
19. Kumar, P. S.; Korving, L.; van Loosdrecht, M. C. M.; Witkamp, G. J. Adsorption as a Technology to Achieve Ultra-Low Concentrations of Phosphate: Research Gaps and Economic Analysis. *Water Research X*. Elsevier: August 1, 2019; p 100029. DOI: 10.1016/j.wroa.2019.100029 .
20. Solscheid, C.; Kunzelmann, S.; Davis, C. T.; Hunter, J. L.; Nofer, A.; Webb, M. R. Development of a Reagentless Biosensor for Inorganic Phosphate, Applicable over a Wide Concentration Range. *Biochemistry* **2015**, *54* (32), 5054– 5062, DOI: 10.1021/acs.biochem.5b00449
21. American Public Health Association (APHA); American Waterworks Association (AWWA); Water Environment Federation (WEF). *Standard Methods for the Examination of Water and Wastewater*; McGraw-Hill Companies, Inc.: New York, NY, U, 2012. .
22. Blaney, L. M.; Cinar, S.; SenGupta, A. K. Hybrid Anion Exchanger for Trace Phosphate Removal from Water and Wastewater. *Water Res.* **2007**, *41* (7), 1603– 1613, DOI: 10.1016/j.watres.2007.01.008
23. Chapra, S. C.; Dove, A.; Warren, G. J. Long-Term Trends of Great Lakes Major Ion Chemistry. *J. Great Lakes Res.* **2012**, *38* (3), 550– 560, DOI: 10.1016/j.jglr.2012.06.010
24. Moussout, H.; Ahlafi, H.; Aazza, M.; Maghat, H. Critical of Linear and Nonlinear Equations of Pseudo-First Order and Pseudo-Second Order Kinetic Models. *Karbala Int. J. Mod. Sci.* **2018**, *4* (2), 244– 254, DOI: 10.1016/j.kijoms.2018.04.001
25. Ho, Y. S.; McKay, G. Sorption of Dye from Aqueous Solution by Peat. *Chem. Eng. J.* **1998**, *70* (2), 115– 124, DOI: 10.1016/S0923-0467(98)00076-1
26. Limousin, G.; Gaudet, J. P.; Charlet, L.; Szenknect, S.; Barthès, V.; Krimissa, M. Sorption Isotherms: A Review on Physical Bases, Modeling and Measurement. *Appl. Geochem.* **2007**, *22* (2), 249– 275, DOI: 10.1016/j.apgeochem.2006.09.010
27. Subramanyam, B.; Das, A. Linearised and Non-Linearised Isotherm Models Optimization Analysis by Error Functions and Statistical Means. *J. Environ. Heal. Sci. Eng.* **2014**, *12* (1), 92, DOI: 10.1186/2052-336X-12-92
28. Du, X.; Li, Y.; Xia, Y. L.; Ai, S. M.; Liang, J.; Sang, P.; Ji, X. L.; Liu, S. Q. Insights into Protein–Ligand Interactions: Mechanisms, Models, and Methods. *Int. J. Mol. Sci.* **2016**, *17* (2), 144, DOI: 10.3390/ijms17020144
29. Brune, M.; Hunter, J. L.; Corrie, J. E. T.; Webb, M. R. Direct, Real-Time Measurement of Rapid Inorganic Phosphate Release Using a Novel Fluorescent Probe and Its Application to Actomyosin Subfragment 1 ATPase. *Biochemistry* **1994**, *33* (27), 8262– 8271, DOI: 10.1021/bi00193a013

30. Tong, Y.; McNamara, P. J.; Mayer, B. K. Adsorption of Organic Micropollutants onto Biochar: A Review of Relevant Kinetics, Mechanisms and Equilibrium. *Environ. Sci. Water Res. Technol.* **2019**, *5* (5), 821– 838, DOI: 10.1039/C8EW00938D
31. USEPA Office of Water Definition and Procedure for the Determination of the Method Detection Limit, Revision 2 *United States Environ. Prot. Agency, Off. Water*2016
32. Ho, Y. S.; McKay, G. Pseudo-Second Order Model for Sorption Processes. *Process Biochem.* **1999**, *34* (5), 451– 465, DOI: 10.1016/S0032-9592(98)00112-5
33. Brune, M.; Hunter, J. L.; Howell, S. A.; Martin, S. R.; Hazlett, T. L.; Corrie, J. E. T.; Webb, M. R. Mechanism of Inorganic Phosphate Interaction with Phosphate Binding Protein from Escherichia Coli. *Biochemistry* **1998**, *37* (29), 10370– 10380, DOI: 10.1021/bi9804277
34. Xiong, W.; Tong, J.; Yang, Z.; Zeng, G.; Zhou, Y.; Wang, D.; Song, P.; Xu, R.; Zhang, C.; Cheng, M. Adsorption of Phosphate from Aqueous Solution Using Iron-Zirconium Modified Activated Carbon Nanofiber: Performance and Mechanism. *J. Colloid Interface Sci.* **2017**, *493*, 17– 23, DOI: 10.1016/j.jcis.2017.01.024
35. Elias, M.; Wellner, A.; Goldin-Azulay, K.; Chabriere, E.; Vorholt, J. A.; Erb, T. J.; Tawfik, D. S. The Molecular Basis of Phosphate Discrimination in Arsenate-Rich Environments. *Nature* **2012**, *491* (7422), 134– 137, DOI: 10.1038/nature11517
36. Missimer, T. M.; Teaf, C. M.; Beeson, W. T.; Maliva, R. G.; Woolschlager, J.; Covert, D. J. Natural Background and Anthropogenic Arsenic Enrichment in Florida Soils, Surface Water, and Groundwater: A Review with a Discussion on Public Health Risk. *International Journal of Environmental Research and Public Health*. MDPI: AG,October 17, 2018. DOI: 10.3390/ijerph15102278 .
37. Lürling, M.; Waajen, G.; Van Oosterhout, F. Humic Substances Interfere with Phosphate Removal by Lanthanum Modified Clay in Controlling Eutrophication. *Water Res.* **2014**, *54*, 78– 88, DOI: 10.1016/j.watres.2014.01.059